Heliyon 10 (2024) e38445

Contents lists available at ScienceDirect

Heliyon

journal homepage: www.cell.com/heliyon

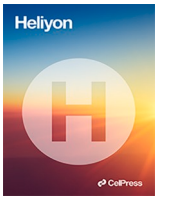

Research article

Mechanism of non-competitive inhibition of the SARS-CoV-2 3CL protease dimerization: Therapeutic and clinical promise of the lichen secondary metabolite perlatolinic acid

Lorenza Fagnani [a], Pierangelo Bellio [a,*], Antonio Di Giulio [a], Lisaurora Nazzicone [a], Roberto Iorio [a], Sabrina Petricca [a], Nicola Franceschini [a], Laura Bertarini [b], Donatella Tondi [b], Giuseppe Celenza [a]

[a] Department of Biotechnological and Applied Clinical Sciences, University of L'Aquila, via Vetoio 1, 67100, L'Aquila, Italy
[b] Department of Life Sciences, University of Modena and Reggio Emilia, Via Campi 103, 41125, Modena, Italy

ARTICLE INFO

Keywords:
SARS-CoV-2 3CL protease inhibition
Perlatolinic acid antiviral activity
Lichen metabolites against COVID-19
3CL protease dimer interface
Broad-spectrum COVID-19 therapeutics

ABSTRACT

In response to the COVID-19 pandemic, identifying effective treatments against SARS-CoV-2 has become of utmost importance. This study elucidates the mechanism by which perlatolinic acid, a lichen-derived secondary metabolite, non-competitively inhibits the dimerization of the SARS-CoV-2 3CL protease, a pivotal enzyme in the virus lifecycle. Utilising a combination of kinetic parameter determination, inhibition assays, and molecular docking studies, we demonstrate that perlatolinic acid effectively disrupts the enzymatic function by binding at the dimer interface with a measured K_i value of 0.67 μM, thereby impeding the protease catalytic activity essential for viral replication. Molecular docking studies further corroborate the binding specificity of perlatolinic acid to the dimer interface, which is attributed to the loss of key interactions essential for dimerization, consequently impairing catalytic activity, highlighting its potential as a scaffold for developing broad-spectrum antiviral drugs.

Despite a dose-dependent cytotoxicity of perlatolinic acid, its TC_{50} is approximately 43 times higher than the K_i value.

Our findings suggest that perlatolinic acid holds significant promise as a lead compound for the development of new therapeutics against COVID-19, warranting further investigation and clinical evaluation.

In conclusion, the study sheds light on the therapeutic potential of natural compounds in combating SARS-CoV-2, paving the way for the exploration of lichen secondary metabolites as a reservoir of potential antiviral agents.

1. Introduction

Severe acute respiratory syndrome (SARS) is a highly contagious and atypical pneumonia infection characterized by cough, high fever, headache, fatigue, shortness of breath, and loss of smell primarily in SARS-CoV-2. In the most severe infections, it may lead to complications such as generalized interstitial infiltrates in the lung, pneumonia, acute respiratory distress syndrome, multi-organ

* Corresponding author.
E-mail address: pierangelo.bellio@univaq.it (P. Bellio).

https://doi.org/10.1016/j.heliyon.2024.e38445
Received 9 April 2024; Received in revised form 20 September 2024; Accepted 24 September 2024
Available online 28 September 2024

failure, and death [1]. As of late 2019, COVID-19 infection caused by a novel severe acute respiratory syndrome coronavirus (SARS-CoV-2) is one of the most threatening pandemic diseases that has become a global health emergency. This recently emerging disease rapidly spread from southern China to different countries around the world [2–6], with 800 million cumulative confirmed infections and about 7 million deaths to date according to the World Health Organization [7]. Coronaviruses (CoVs) have been known since 1947 when the prototype murine JHM strain was reported [8]. As in other respiratory viruses, the transmission occurs through larger droplets upon coughing and sneezing [9].

Before the emergence of SARS-CoV-2, six different of coronaviruses were known to infect humans: HCoV-229E, HCoV-OC43, HCoV-NL63, HCoV-HKU1, SARS-CoV, and MERS-CoV. The first four strains are responsible for mild respiratory diseases, while the last two have caused severe respiratory epidemics. They belong to the subfamily *Orthocoronavirinae* of the family *Coronaviridae*, which is part of the order *Nidovirales*. Coronaviruses are characterized by an envelope and the largest positive-stranded RNA viral genome, ranging from 26 to 32 kb [10]. They have been divided into four genera (α-, β-, γ-, and δ-coronaviruses): α- and β- CoVs infect mammals, γ-CoVs infect avian species, and δ-coronaviruses infect both mammals and avian species [8]. SARS-CoV, MERS-CoV and SARS-CoV-2 belong to the β-coronaviruses [11]. All three CoVs are zoonotically transmitted and spread among humans through close contact. The genome of SARS-CoV-2 shares about 82 % sequence similiarity with SARS-CoV and 50 % with MERS-CoV and more than 90 % sequence identity for essential enzymes and structural proteins [12]. This high degree of shared genetic sequence has resulted in a common pathogenetic mechanism.

The SARS-CoV-2 genome is organized into 14 ORFs encoding structural, non-structural, and accessory proteins [13]. The first ORF (ORF 1a/b) translates into two polyproteins, which are then transformed into 16 non-structural proteins by 3CL protease [14]. Non-structural proteins play a key role during the virus life cycle, while the spike glycoprotein is required for virus interactions with host cell receptors during virus entry. These non-structural proteins are processed by two cysteine proteases encoded by ORF1a, the papain-like protease PL^{pro} and the major protease $3CL^{pro}$. PL^{pro} cuts the first three cleavage sites of its polyprotein, while $3CL^{pro}$ cuts the remaining 11 sites, releasing 15 non-structural proteins [8]. PL^{pro} and $3CL^{pro}$ play the same role in SARS and MERS-CoV.

Coronavirus $3CL^{pro}$ is a cysteine protease composed of 306 amino acids and consists of two monomers forming a dimer. Each monomer possesses three domains, *N*-terminal, central, and *C*-terminal, and a catalytic dyad (Cys145-His41) between domains I and II. The $3CL^{pro}$ monomers of SARS-CoV-2 are enzymatically inactive, as the protease is active as a homodimer [8]. The dimerization is crucial for the catalytic activity of the enzyme as a result of the interaction of amino acid residues from both subunits. The high mobility of the *C*- and *N*-terminus of the monomer form are tightly held when the dimer is formed [8]. $3CL^{pro}$ is pivotal for viral replication, so its inhibition can be exploited as a valuable strategy for blocking viral RNA replication and transcription, thereby preventing viral proliferation. In addition, $3CL^{pro}$ represents a promising target for developing broad-spectrum therapeutic agents because of its highly conserved three-dimensional structure among the different coronaviruses, for example, SARS-CoV and MERS-CoV. Since humans do not possess a homologous version, inhibiting the viral 3CL protease represents a suitable strategy for developing potential antiviral drugs.

The SARS-CoV-2 epidemic and its associated consequences worldwide have prompted the scientific community to develop potential drugs to combat COVID-19 [1,14]. Although various treatment strategies such as azithromycin, chloroquine derivatives, and convalescent plasma have been explored [8], and specific antiviral drugs like Paxlovid have been approved [15], the ongoing research continues to seek out new and potentially more effective antiviral therapies.

Two suitable approaches for developing inhibitors against this enzyme are (i) blocking the catalytic activity and thus targeting the substrate binding pocket and (ii) dimerization inhibition. Most of the scientific literature on this theme is based on designing inhibitors that target the substrate-binding pocket. However, to date, no such inhibitors have reached clinical trials. Although there are a few reports in the scientific literature on inhibitors that target SARS-CoV M^{pro} dimerization, it represents an attractive therapeutic strategy [16].

A valuable alternative to the lack of potential drugs can be found in natural compounds. Due to their promising efficacy, natural compounds are uften used for research and therapy [9]. In particular, lichen compounds can be considered a natural and valuable treasure for antibacterial and antiviral drug candidates [17,18]. Numerous lichen species have been reported to have antiviral, antifungal, and antibacterial activities [2,18], besides having antiproliferative, antioxidant, analgesic, anti-inflammatory, and antipyretic properties [9]. In this study, we addressed our investigations on the potential inhibitor activity of lichen secondary metabolites on SARS-CoV-2 3CL protease, focusing on perlatolinic acid (Fig. 1).

Perlatolinic acid, obtained from *Stereocaulon* sp., is a natural compound belonging to the class of depsides. A recent study

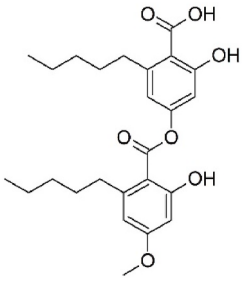

Fig. 1. Structure of perlatolinic acid.

demonstrated the antiviral activity of perlatolinic acid against SARS-CoV-2 [19]. In consideration of the urgent need to address an efficacious answer to the pandemic [20] and our previous study in which salazinic acid and protocetraric acid, two secondary lichen metabolites, have been proven to be competitive inhibitors of 3CL [21], we further investigate the inhibitory activity the perlatolinic acid against 3CL, in order to clarify the possible mechanism of the demonstrated antiviral action [19].

2. Results

2.1. Determination of kinetic parameters

The kinetic parameters for the $3CL^{pro}$ enzyme were determined by plotting the initial velocity (v_0) versus substrate concentration, which is described by the Hill equation for a cooperative enzyme, as previously reported [20]. The results indicate that the enzyme exhibited a V_{max} value of 2831 ± 174 RFU s^{-1} (RFU, Relative Fluorescence Unit) corresponding to 0.0149 μM s^{-1} with a k_{cat} value of 2.84 s^{-1}. The enzyme-substrate affinity, K, was determined to be 43.2 ± 4.8 μM, and the Hill coefficient, h, was calculated as 1.37 ± 0.02. The non-Michaelian behaviour was confirmed by applying the Hanes-Woolf linearization of the Michaelis-Menten equation as suggested in previous work [20].

2.2. Inhibition assay

The time-course plots were determined at several concentrations of perlatolinic acid, ranging from 0.5 μM to 50 μM. As shown in Fig. 2, the time courses are consistent with a slow-binding inhibition mechanism. The slow-binding nature exhibits a time-dependent binding process characterized by a slow association rate. This means that the binding equilibrium between the inhibitor and the enzyme on a time scale is slower with respect to the turnover rate of the enzyme-catalyzed reaction [21].

A crucial aspect requiring elucidation is the determination of the mechanism of inhibition, which is initially addressed through a detailed analysis setting different DynaFit scripts to assess the hypothetical models of inhibition: competitive, non-competitive, un-competitive, and mixed types. The outcomes of our investigation demonstrate a plausible non-competitive inhibition model, which is substantially supported by the observed experimental data.

The results of k_{on} and k_{off} values were reported in Table 1. The value of the constant of inhibition (K_i) has been determined as the ratio between the k_{off} and k_{on}.

Non-competitive inhibitors can bind the free enzyme and the Michaelis complex, potentially affecting the K_m and/or the V_{max} values in dependence on the α value (equation (2)).

The α value has been experimentally determined by evaluating the kinetic parameters both in the presence and absence of the inhibitor. This was made by plotting the initial velocity (v_0) versus different substrate concentrations, both in the absence of perlatolinic acid and with a fixed inhibitor concentration of 25 μM (Fig. 3A and B).

In our case, the non-competitive inhibition involves a decrease in the values of V_{max} while the K value remains unchanged. In detail, the K parameter remains nearly unaltered, with a value of about 40. V_{max} value exhibits a reduction in the presence of the inhibitor (1932.88 ± 31.51 RFU s^{-1} instead of 2831.13 ± 174.05 RFU s^{-1}). This aligns with the characteristics of a non-competitive inhibitor with $\alpha = 1$, in which K remains unchanged. At the same time, V_{max} is affected, leading to the conclusion that perlatolinic acid can indifferently bind the free enzyme E and the Michaelis complex (ES).

Moreover, the results suggest that the enzyme exhibits comparable behaviour regardless of the presence and absence of perlatolinic acid. Furthermore, it is noteworthy that the 3CL protease maintains its cooperative behaviour, regardless of the presence of the lichen

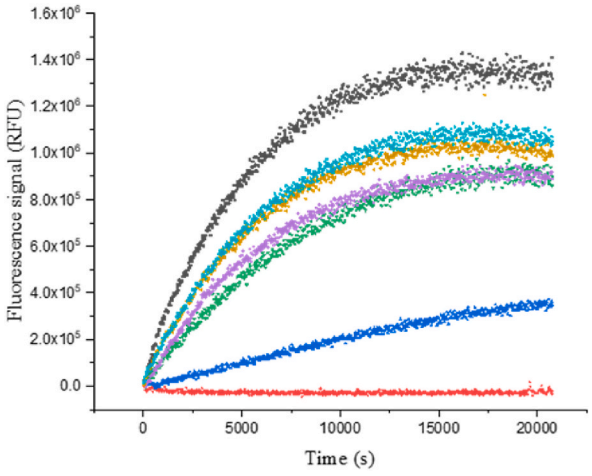

Fig. 2. Time-course plots at different inhibitor concentrations. Black, positive control; red, perlatolinic acid 50 μM; blue, 25 μM; green, 10 μM; magenta, 5 μM; yellow, 1 μM; light blue, 0.5 μM.

Table 1
Estimation of inhibition parameters at 10 μM of substrate.

Compound	k_{on}	k_{off}	K_i (μM)
Perlatolinic acid	$4.56 \times 10^{-5} \pm 8.7 \times 10^{-7}$	$3.04 \times 10^{-5} \pm 1.7 \times 10^{-6}$	0.67

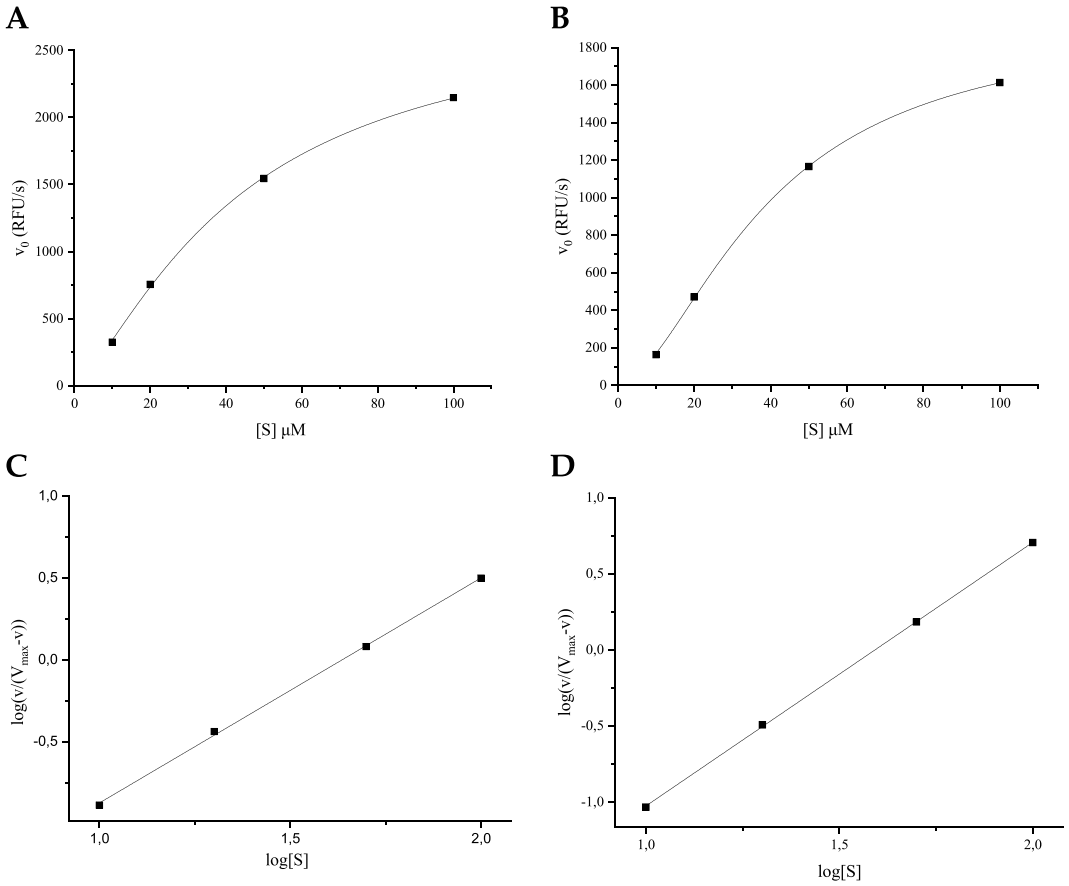

Fig. 3. The plot of the initial velocity (v_0) versus substrate concentrations both in the absence (**A**) and presence (**B**) of the inhibitor. **C, D**: The linearization of the Hill equation by plotting *log(v/(V$_{max}$-v))* as a function of *log[S]*.

compound.

The velocity data for cooperative enzymes can be presented in a linear form by graphing equation (1):

$$\log \frac{v}{V_{max} - v} = h \log[S] - \log(K) \tag{1}$$

Thus, a plot of *log(v/(V$_{max}$-v))* versus *log[S]* should produce a straight line with a slope of *h* and a *y*-intercept of *-log(K)*. The verification of our results is obtained with R^2 values almost close to 1, specifically 0.99988 for [I] at 25 μM (Fig. 3C) and 0.99935 without perlatolinic acid (Fig. 3D). The slope of the straight line provides an estimate of the Hill coefficient *h*, a value of 1.37 ± 0.02 in the absence of perlatolinic acid and 1.73 ± 0.01 with a concentration of 25 μM of inhibitor.

2.3. Molecular docking

Docking studies were carried out to clarify further the molecular mechanism of inhibition of SARS-CoV 3CL^{pro} by perlatolinic acid. Given the absence of 3CL^{pro}-noncompetitive inhibitor crystal complexes, a SiteMap analysis of the protein was conducted to determine the target protein accessible binding site for docking studies. This preliminary analysis identified four available binding sites (Fig. 4), including shallow ones, whose scores and volumes are reported and ranked in Table 2. According to SiteScore, the two best sites, Site 1 and Site 2, cover some of the critical residues involved in dimerization and were selected for grid generation and docking. The coordinates of the primary sites, specifically site 1 and site 2, are provided in PDB format. In agreement with the findings of the kinetics analysis, Site 3 was excluded, despite the promising score, as it covered the catalytic dyad His41-Cys145. Site 4 was not further

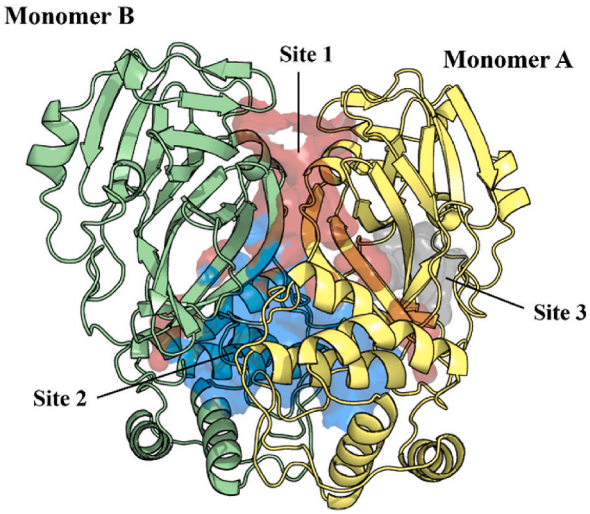

Fig. 4. Representative structure of $3CL^{pro}$ dimer with the three main predicted binding sites: Site 1 (red), Site 2 (blue), and Site 3 (grey). Site 4 is not included. The protein is shown in cartoons (Chain A in pale yellow and Chain B in pale green) and sites as Connolly surfaces.

Table 2
Sitemap analyses for $3CL^{pro}$. Sites are ranked according to SiteScore.

Site	SiteScore	DScore	*Volume*
Site 2	0.998	1.012	1608.756
Site 1	0.986	1.001	1721.560
Site 3	0.983	1.008	444.056
Site 4	0.546	0.497	35.372

investigated due to its poor score and size.

Therefore, a preliminary set of rigid docking simulations was performed in SP and XP modes in the two selected sites to assess the binding mode and affinity of the ligand. Interestingly, perlatolinic acid showed a significantly lower score and better accommodation into Site 2, located at the interface between the two monomers, while for Site 1, worse docking scores and a higher variability between poses were reported (Fig. 5).

Given the promising druggability of Site 2 and low docking scores obtained, perlatolinic acid was sent to Induced Fit docking simulations against Site 2, thus helping to predict ligand binding modes and concomitant structural changes in the target protein complex. Overall, for the predicted enzyme-inhibitor complex, binding was guided by the interaction with Arg4 and Lys5 residues, known to be crucial for enzyme dimerization and, thus, catalytic activity [16,22,23]. The ligand was further stabilized by specific interactions such as hydrogen bonds, salt bridges, and π–cation interactions, ensuring suitable accommodation and steric complementarity within the binding site. Noteworthy is the binding at the dimer interface, which involves residues belonging to each monomer, and despite the different ligand orientations and the flexibility of the amino acid chains, the residues involved turn out to be

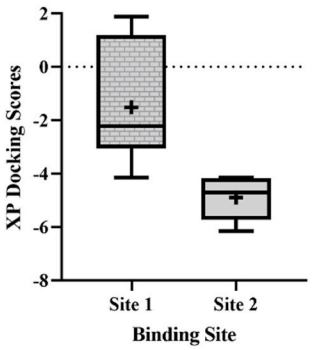

Fig. 5. Docking scores from the XP protocol for the two selected binding sites. Each box plot indicates the median value (black line), mean value ("+" symbol), and first and last quartile, whereas the whiskers span from minimum to maximum. The box plot graph was generated using GraphPad Prism 9 (GraphPad Software, La Jolla, CA, USA).

constant across poses.

In the binding prediction for perlatolinic acid, the phenolic ring H-bonds to Glu288B and establishes further π-cation interaction with Arg4A. Moreover, the carboxylic group creates an H-bond/salt bridge network by interacting with Arg4B, Lys5A and the backbone of Lys5B, thus involving both monomers in ligand stabilization (Fig. 6). Additional hydrophobic interactions between the two flexible alkyl chains and Phe3, Phe291 and Glu288 side chains, belonging to both monomers, contribute to ligand accommodation and display symmetry in ligand binding. Moreover, the aromatic carboxyl ring is stabilized by apolar contacts with both Lys5 (Figure * SI). Perlatolinic acid affinity for the dimer interface is further supported by a consistently low docking score (−9.035 kcal/mol).

To assess the structural changes induced by ligand binding, "pre" and "post docking simulations" proteins were superimposed. Following the non-competitive mechanism of inhibition, no changes were observed at the catalytic site level, thus allowing substrate accommodation. On the contrary, the binding of perlatolinic acid induced a rearrangement of the residues located at the interface of the dimer to ensure a better fit and an increased stabilization of the ligand. However, such changes resulted in the loss of key interactions between Arg4B-Glu290A and Ser139B-Gln299A, H-bonds and salt bridges, which have been demonstrated to be crucial for dimer formation and its catalytic activity [22,24].

2.4. Cell culture and viability assay

The trypan-blue exclusion assay demonstrated a dose-dependent cytotoxicity elicited by perlatolinic acid on TM4 cells at the tested doses, ranging from 0 to 80 μM, after exposure for up to 48 h (Fig. 7). The results show an TC_{50} value of 37.7 ± 1.81 and 26.1 ± 0.78 for 24 and 48 h of exposure, respectively.

3. Discussion

Since the beginning of the pandemic, the potential of natural products as effective 3CL protease inhibitors of SARS-CoV-2 has been one of the most explored fields of investigation, as the enormous diversity of the chemical space of naturally occurring substances may provide molecular scaffolds for the development of viral protease inhibitors. Intensive research in this field has been mainly carried out through virtual screening and dynamic simulations of large libraries [25–28] leading to the identification of natural products virtually capable of binding to the 3CL active site. Our previous work demonstrated how protocetratic acid and salazinic acid, secondary metabolites from lichens, can competitively inhibit 3CL protease [20]. In this study, we focused on perlatolinic acid, a lichen secondary metabolite belonging to the class of depsides. Nevertheless, the catalytic site does not represent the only enzymatic target. For instance, it has been extensively demonstrated that the 3CL enzymatic function depends on dimerization, which occurs upon substrate binding followed by a structural change that leads to activation. A study by Wang et al. [29] explored the impact of a naturally occurring G11S mutation in the 3C-like protease from the SARS-CoV-2 virus on the dimer interface. Their findings suggest that targeting the dimer interface with inhibitors could be an effective strategy, especially considering the emergence of SARS-CoV-2 variants. This study emphasizes the necessity for inhibitors that can destabilize the 3CL dimer, hindering its function. The research highlights the significance of protein-protein interaction (PPI) inhibitors in addressing this mechanism. It is not by chance that recent studies have illuminated the potential of targeting the dimer interface of the 3CL protease in SARS-CoV-2 for therapeutic intervention. One

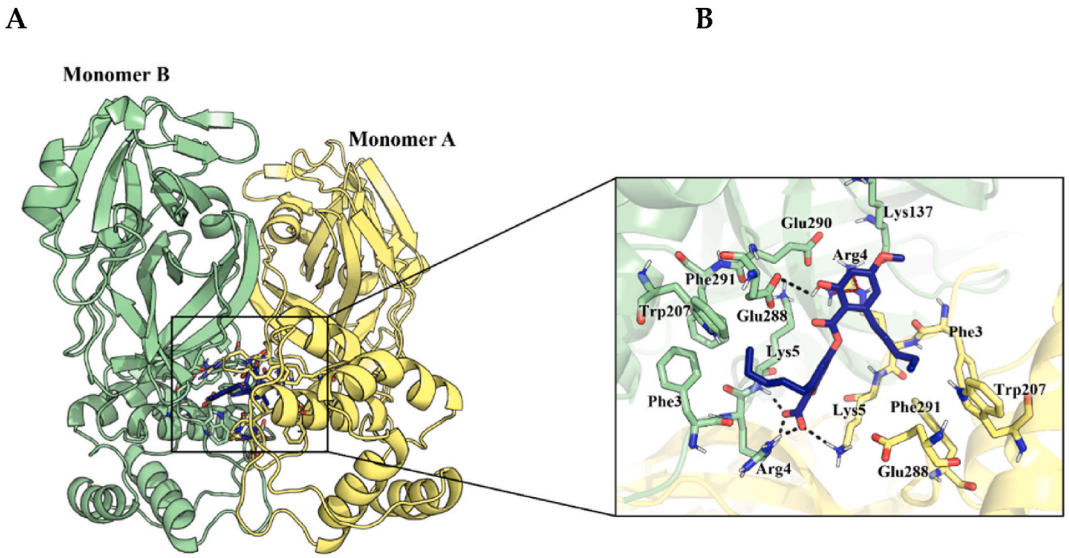

Fig. 6. A. Representative structure of $3CL^{pro}$ dimer with docked ligand. B. Docking pose of Perlatolinic Acid (blue) at the dimer interface, from Induced Fit protocol. The protein is shown in cartoons (Chain A in pale yellow and Chain B in pale green); the ligand (blue) and the residues lining the pocket are displayed in capped sticks. Hydrogen bonds (black) and π-interactions (red) are shown as dashed lines.

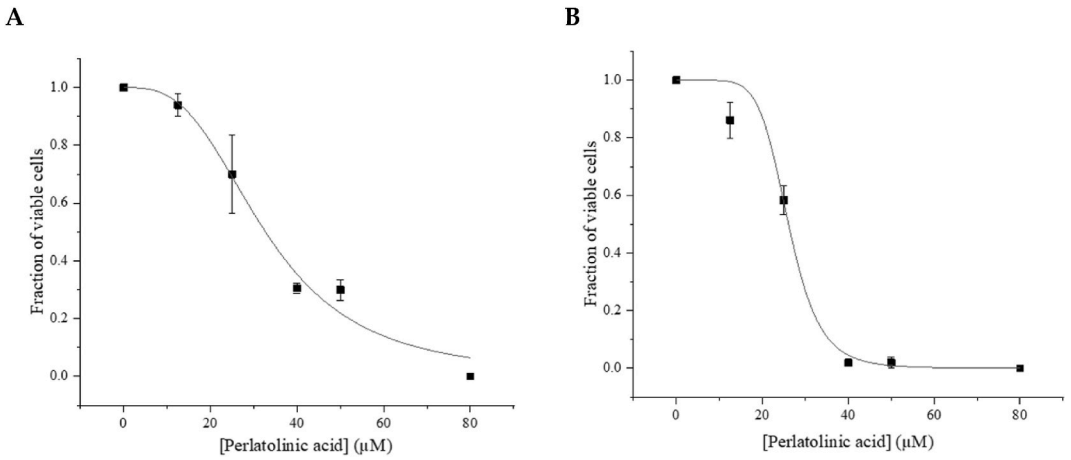

Fig. 7. Cell culture and viability assay, with exposure up to 24 h (A) and 48 h (B).

significant aspect of this approach is the ability of certain inhibitors to bind at this interface, disrupting the enzymatic activity crucial for viral replication. Investigations have discovered that certain natural compounds can act as inhibitors of 3CL dimerization, for example, extract from *Ginkgo biloba* [30], *Aloe* spp [31]. or *Citrus japonica* [32]. These studies collectively suggest a non-competitive mechanism of inhibition, where natural product inhibitors bind to allosteric sites on the 3CL protease. This mode of action, distinct from the active site, induces conformational changes in the enzyme, impairing its function without directly competing with the substrate. Such non-competitive inhibition is particularly promising as it offers a strategic advantage in circumventing viral mutation-induced resistance, a common challenge in antiviral drug development. Based on the results obtained, we can propose a general reaction scheme that illustrates, as experimentally demonstrated, a non-competitive inhibition mechanism (Scheme 1).

As previously described [16], the $3CL^{pro}$ primarily exists in a monomer-dimer equilibrium with a dissociation constant (K_d) of approximately 6 μM. As known in literature [22], $3CL^{pro}$ exhibits weak dimerization in the absence of substrate. However, substrate-induced dimerization is crucial for its enzymatic activity. As evidenced by previously studies [16,22,33], substrate binding significantly enhances and stabilizes the dimer formation, which is essential for the catalytic function of the protease. The binding of the substrate to the inactive monomeric form (M) of the 3CL entails a conformational change, which leads to the formation of the active enzyme. In the general reaction scheme, the binding of S to the non-active monomer (M) to form the Michaelis complex generates the active form of the enzyme (E). However, due to the lack of more detailed knowledge, the transition from the encounter form of the monomers with the substrate to the Michaelis complex (ES) is not relevant for the comprehension of the inhibition mechanism and, therefore, was considered a "black box". It is hypothesized that the allosteric information acquired due to the binding of the substrate to the monomeric form, which leads to the formation of the active enzyme (E), is not immediately lost once the catalytic cycle is initiated. This allows the "E state" to persist for the time required to initiate a new catalytic cycle. In terms of rate constants, this translates to a value of k_{+4} being approximately equal to, or slightly greater than, k_{-3}. While the formation of an ESI complex is relatively straightforward, elucidating the formation of an EI complex remains more challenging. As extensively demonstrated in the literature and previously reported, dimer formation results from substrate binding. The hypothesis of the persistence of an "E state" with the catalytic cycle underway explains this paradox. Indeed, under steady-state conditions, considering k_{+4} roughly equal to k_{-3}, which we can define as the "E persistence condition," the binding of the inhibitor at the monomer interface becomes plausible. This model aligns well with a non-competitive inhibition mechanism with an *alpha* value of 1, a conclusion confirmed by the *in-silico* simulation where the inhibitor is located at the interface between the two monomers. The results of the *in-silico* analysis are

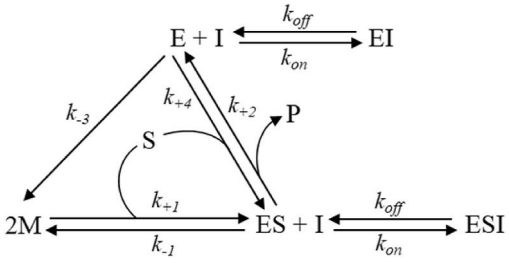

Scheme 1. General reaction scheme illustrating the mechanism of non-competitive inhibition of perlatolinic acid. The kinetic mechanism involves the interactions of the enzyme (E) with the substrate (S) and the inhibitor (I). It describes the formation of the enzyme-substrate complex (ES), the enzyme-inhibitor complex (EI) and the enzyme-substrate-inhibitor complex (ESI), as well as the formation of the product (P). The various rate constants governing the transitions between these states are referred to as k_{on}, k_{off}, k_{+1}, k_{-1}, k_{+2}, k_{+4}, *and* k_{-3}.

subsequently discussed in greater detail. As previously stated, the mechanism of substrate binding to the monomers and the subsequent formation of the active enzyme in the Michaelis complex (ES) conformation has not yet been fully elucidated. However, this may be considered irrelevant when interpreting the results. Noteworthy is that the 3CL protease maintains its cooperative behaviour regardless of the presence of the lichen compound. The maintenance of cooperative behaviour leads us to assume that perlatolinic acid preferentially binds the enzyme after dimer formation. *In-silico* studies demonstrate the ability of perlatolinic acid to complement the site located at the dimer interface without disturbing the active site and symmetrically binding to both monomers. In our study, perlatolinic acid was subjected to Induced Fit docking simulations against the dimer interface. The low docking scores obtained and the predicted binding modes suggest a strong affinity of perlatolinic acid for this site. The binding interactions are primarily guided by Arg4 and Lys5, residues that are essential for enzyme dimerization and, therefore, for its catalytic activity. Our study further elucidates that the binding of perlatolinic acid at the dimer interface involves residues from both monomers, indicating a symmetrical binding pattern crucial for its inhibitory action. The binding of perlatolinic acid to Glu288B and Arg4A, and the formation of an H-bond/salt bridge network with Arg4B, Lys5A, and Lys5B, demonstrate the complex interaction network at the dimer interface. This network is essential for the stability and accommodation of the ligand, leading to the disruption of key interactions necessary for dimer formation. Our study on perlatolinic acid and its binding to the dimer interface of the 3CL enzyme complements the findings of Wang et al. [29], who discovered that a Gly to Ser mutation at the interface significantly destabilizes the dimer, reducing its stability by approximately 600-fold. Furthermore, our study confirms the non-competitive inhibition mechanism of perlatolinic acid, as no significant changes were observed at the catalytic site level post-ligand binding, allowing substrate accommodation. This is particularly relevant in light of Wang et al.'s findings, as it suggests that effective inhibitors can target the dimer interface without directly interfering with the active site but decreasing the enzyme stability. An important aspect of our findings is the relatively mild cytotoxicity associated with perlatolinic acid if compared to the K_i value. For instance, the cytotoxicity data on epithelial TM4 cells are compelling, as this natural compound shows an TC_{50} value approximately 43 times higher than its K_i value. This significant disparity highlights the potential therapeutic efficacy with minimal cytotoxic effects of perlatolinic acid, making it a promising natural candidate for further development. In addition, its cytotoxicity aligns with the broader trend observed in lichen-derived compounds, often recognized for their bioactive properties with minimal adverse effects on human cells [34–36]. This characteristic is particularly noteworthy, as it suggests a favourable safety profile for lichen secondary metabolites, making them promising candidates for therapeutic applications. The ability of perlatolinic acid to inhibit the 3CL protease of SARS-CoV-2, combined with its low cytotoxicity, underscores its potential as a viable antiviral agent. A recent study investigated the antiviral activity of several natural compounds, of which 28 were secondary lichen metabolites [19]. The perlatolinic acid was found to be the most active against alpha and betacoronaviruses, HCoV-229E and SARS-CoV-2, respectively. It is interesting to highlight that the authors demonstrated that perlatolinic acid inhibits the replication of the viruses. It is not by chance that the 3CL protease is involved in the replication process. Therefore, the favourable safety profile and the antiviral activity of this natural compound present a significant advantage in drug development, potentially reducing the time and resources required for clinical trials and hastening the availability of effective treatments against viral infections like COVID-19. Further studies must be addressed better to exploit the enormous resource of lichen secondary metabolites.

4. Limitations of the study

This study explores the efficacy of perlatolinic acid, a secondary metabolite from lichens, in inhibiting the dimerization of the SARS-CoV-2 3CL protease, highlighting its potential as an antiviral agent. Despite promising results obtained through molecular docking approaches, kinetic assays, and cell culture analyses, there are several limitations that require further investigations. Firstly, the generalizability of the results to the human clinical context remains uncertain since, before being considered for human trials, the compound needs to be evaluated in different animal models. Differences between *in vitro* systems and living organisms, including the complexity of metabolism and interaction with the immune system, could affect the efficacy and safety of perlatolinic acid. Therefore, comprehensive clinical studies are essential to confirm its therapeutic potential. Secondly, the research does not address the risk of long-term viral resistance development, a critical aspect for assessing the sustained efficacy of the antiviral. Similarly, potential toxicities and side effects that might emerge with higher dosages or prolonged treatments have not been detailed. Moreover, the specificity of perlatolinic acid action, its efficacy against mutated viral variants, and the scalability of production represent further challenges. Although the study provides a promising basis for the use of perlatolinic acid as an antiviral against SARS-CoV-2, it highlights the need for more comprehensive research.

5. Materials and methods

5.1. Reagents

SARS-CoV-2 3CL Protease was purchased from Sigma-Aldrich/Merck KGaA. 3CL Protease Substrate, 3CL Protease Assay Buffer, and 3CL inhibitor GC376 were purchased from Vinci Biochem (Firenze, Italy). Dithiothreitol (DTT) and dimethyl sulfoxide (DMSO) were purchased from Sigma-Aldrich Chemical Co. (Saint Louis, MO, USA). Dulbecco's modified Eagle medium (DMEM)/Ham's F-12 50/50 Mix (with 2 mM L-glutamine and 15 mM Hepes) was purchased from Corning Life Sciences (Manassas,VA, USA). Fetal bovine serum (FBS), and horse serum (HS) were from EuroClone (Pero, MI, Italy). Penicillin-streptomycin was from TermoFisher Scientific (Carlsband, CA, USA). Trypan-blue assay and other reagents were from Sigma-Aldrich Chemical Co. (Saint Louis, MO, USA). Perlatolinic acid (Fig. 1), isolated from lichens collected in various Chilean regions, including the Chilean Antarctic Territory, was donated by Prof. Marisa Piovano (Universidad Técnica Federico Santa María, Valparaíso, Chile). The purity of the perlatolinic acid was higher

than 98 %, as previously determined by HPLC [37].

5.2. Spectrofluorimetric assay

SARS-CoV-2 3CL protease activity assay was used to assess the effect of lichen secondary metabolites on inhibiting the 3CL protease. With some modifications, the assay was performed according to the manufacturer's protocol (3CL Protease (SARS-CoV-2) Assay Kit, BPS Bioscience). The fluorescence intensity was measured using the fluorogenic substrate DABCYL-KTSAVLQSGFRKME-EDANS, in a microtiter plate-reading fluorimeter capable of excitation at a wavelength of 360 nm and detection of emission at a wavelength of 535 nm.

Reactions were performed in a black 96-well microplate with a final volume of 100 μL in each well, as previously described [21]. The reaction buffer used for the experiments requires the addition of dithiothreitol (DTT) 1 mM to preserve the enzyme integrity due to the long-run experiments. DTT was added to 3CL Protease Assay Buffer just before use. 3CL protease was used at the final concentration of 8.9 nM. The reaction was started by adding the 3CL substrate to each well at a concentration value of 10 μM, as previously described [20].

The spectrofluorimetric assay was performed by measuring the fluorescence intensities in each well using the Beckman Coulter DTX-880 Multimode Detector microplate reader. The excitation and emission wavelengths were 360 nm and 535 nm, respectively. The percentage of inhibition was calculated as the fractional residual activity of protease 3CL incubated for 30 min with the lichen compound. The inhibitor buffer was used as a negative control, while the 3CL inhibitor GC376 with a concentration of 100 μM was used as a positive control.

A standard curve was produced to convert the relative fluorescence unit (RFU) into the amount of cleaved substrate. The curve was obtained by inducing complete hydrolysis of the substrate with concentrations ranging from 5 to 100 μM, as previously demonstrated by Fagnani et al. [20].

5.3. Determination of kinetic parameters

The kinetic parameters of 3CL SARS-CoV-2 protease were determined by incubating the enzyme as previously described. The experiment was performed by measuring the initial rates (v_0, RFU/s) of the progress curves calculated at less than 10 % hydrolysis of the initial substrate concentration. The substrate concentrations used in the experiments range from 10 μM to 100 μM.

The plot was well described by the non-linear fitting of the Hill equation:

$$v_0 = \frac{V_{max}[S]^h}{(K)^h + [S]^h}$$

Any deviation from the Michaelis-Menten equation, where h is equal to 1, can be confirmed by the Hanes-Woolf linearization method, in which the initial rate v_0 is plotted as $[S]/v_0$ against [S], as described by Fagnani et al. [20]. Briefly, when h is equal to 1, the plot is illustrated by a straight line with a coefficient of determination R^2 of the interpolated line close to 1. Otherwise, when h is different from 1, R^2 is far from 1.

5.4. Inhibition assay and determination of the mechanism of inhibition

The inhibition assays were performed at different inhibitor concentrations, ranging from 0.5 μM to 50 μM (Fig. 2). The experiments were conducted in a black 96-well microplate, as mentioned above.

The mechanism of inhibition for perlatolinic acid was first determined through the software package DynaFit [38], using different modes of inhibition. Equation (2) was used to determine the α value to identify the binding site of perlatolinic acid.

$$v = \frac{\frac{V_{max}}{\left(1+\frac{[I]}{\alpha K_i}\right)}[S]}{[S] + K_m\left(\frac{\left(1+\frac{[I]}{K_i}\right)}{\left(1+\frac{[I]}{\alpha K_i}\right)}\right)} \quad (2)$$

The theoretical model was experimentally confirmed by assessing the kinetic parameters, in particular V_{max} and K, in the presence and absence of perlatolinic acid, achieved by plotting the initial velocity (v_0) versus substrate concentrations (Fig. 3A and B). The experimental setup involved a series of substrate concentrations (10, 20, 50, and 100 μM) while maintaining perlatolinic acid at a fixed concentration of 25 μM.

The cooperative behaviour of the 3CL protease was ascertained through the linearization of the Hill equation by plotting $log(v/(V_{max}\text{-}v))$ as a function of $log[S]$ (Fig. 3C and D) in the presence of perlatolinic acid at a concentration of 25 μM and in its absence. R^2 and h values were also determined.

5.5. Molecular docking

Perlatolinic Acid was submitted to docking calculations towards $3CL^{pro}$ to investigate its binding mode and the major receptor-ligand interactions. Crystallographic structures of SARS-CoV-2 and SARS-CoV $3CL^{pro}$ available in Protein Data Bank (PDB) (https://www.rcsb.org/) were collected and ranked according to resolution, structure integrity and the presence of a co-crystallized ligand. Both SARS-CoV and SARS-CoV-2 were considered as they show 96 % sequence identity, with only 12 variant residues out of 306, none of them involved in any major roles in the enzymatic activity of the protein [16]. Given the non-competitive inhibition of perlatolinic acid, the research has been narrowed to targets co-crystallized with inhibitors within the active site. For this purpose, the X-ray structure of the SARS-CoV main protease covalently bound to indole Chloropyridinyl Ester-Derived inhibitor (PDB ID: 7RC1) was selected [39]. Before docking, the protein structure was prepared while using the Protein Preparation Wizard in Maestro (Schrödinger LLC suite, version 2022–2, NY, USA), ionized at a pH of 7.4 using PROPKA, minimized using the OPLS4 force field and converging the heavy atoms to a RMSD of 0.30 Å. Water molecules, metals and the cognate ligand were removed. Perlatolinic acid was built via 2D sketcher panel in Maestro, then it was submitted to ligand preparation by LigPrep module, including conversion of 2D structure to 3D ones, hydrogens addition, partial charges computation and structure optimization at a pH of 7.0 ± 2.0 using Epik.

To predict the target druggability and identify the potential allosteric binding sites, the prepared protein was submitted to SiteMap (SiteMap, Schrödinger, LLC, New York, NY, 2022), looking for binding sites on the entire protein structure, including shallow sites. The definition of hydrophobicity used in the calculation was set to "more restrictive", and a fine grid was selected. Binding sites were then selected from all identified sites, and all output values were recorded.

Having identified the top-ranked binding sites, perlatolinic acid was submitted to docking simulations. In the rigid docking mode, the grid was generated and centred on the binding site from SiteMap calculations; the Receptor Grid Generation module was carried out with default parameters, while serines 139, 144 and 147 were set as rotatable. The ligand was then docked both with Glide SP and XP protocol. In order to further investigate the binding mode of the ligand and allow a certain degree of flexibility at the dimer interface, perlatolinic acid was docked in an induced-fit mode (Induced Fit Docking protocol; Glide, Schrödinger, LLC, New York, NY, 2022; Prime, Schrödinger, LLC, New York, NY, 2022). The grid was centred on Arg4, Lys5, Lys137 and Glu288, residues lining the pocket previously identified by SiteMap. The extra-precision (XP) protocol was adopted using a maximum number of poses equal to five, refining residues within 5.0 Å of ligands and automatically trimming the side chains based on B-factor.

5.6. Cell culture and viability assay

TM4 (ATCC® CRL1715™) mouse Sertoli cells were purchased from the American Type Culture Collection.

Cells were initially seeded at a density of 1×10^4 cells/cm^2 and regularly cultured in DMEM/F-12 50/50 Mix supplemented with 5 % HS (horse serum), 2.5 % FBS (fetal bovine serum), 100 IU/mL penicillin, and 100 μg/mL streptomycin until they reached a confluence of about 80 %. Proliferation and viability rates were evaluated using a Trypan blue exclusion assay. Cells were maintained at 37 °C in a humidified atmosphere containing 5 % CO_2. Cells were seeded at a density of 1×10^4 cells/cm^2 and maintained under standard conditions for 24 h before treatments. Afterwards, cells were exposed to perlatolinic acid at concentrations ranging from 0 to 80 μM for 24 and 48 h (Fig. 7).

5.7. Statistics and data analysis

All experiments were performed in triplicate. The parameters, experimental errors, and non-linear fitting were assessed and calculated using Microsoft Excel and OriginPro 8.5.1. The analysis concerning the kinetic inhibition parameters was conducted using the software DynaFit ver 4.09.047 b y Petr Kuzmic (BioKin Ltd.). The modelling analysis was performed with Schrödinger LLC suite, version 2022–2, NY, USA. Figures were generated using Pymol (Pymol Molecular Graphics System, Version 2.0 Schrödinger, LLC).

6. Conclusions

The intensive research conducted since the onset of the COVID-19 pandemic has significantly advanced our understanding of the 3CL protease of SARS-CoV-2, a critical target for antiviral therapy. Our study underscores the promising potential of natural products as effective inhibitors of this enzyme. The discovery of perlatolinic acid, a natural compound from lichens, as a potent non-competitive inhibitor targeting the dimer interface of the 3CL protease, represents a significant step forward in developing novel therapeutic strategies against SARS-CoV-2.

Our findings demonstrate that perlatolinic acid binds effectively to the dimer interface, disrupting key interactions necessary for the formation and stability of the enzymatic dimer. This mode of action aligns with the need for innovative approaches to overcome viral mutation-induced drug resistance, circumventing potential resistance mechanisms that often arise with active site-targeted drugs.

In light of these findings, our study contributes to the growing body of research that seeks to exploit the diversity of natural compounds to develop effective and safe treatments against SARS-CoV-2. As the world continues to grapple with the challenges posed by COVID-19 and other emerging viral threats, the findings from studies such as ours highlight the crucial role of innovative scientific research in paving the way for effective and resilient therapeutic solutions.

Moreover, our research contributes to the growing interest in exploring lichen secondary metabolites as a source of new, safe, and effective antiviral agents, further highlighting the importance of natural products in the ongoing fight against emerging viral diseases.

Data availability statement

Data will be made available on request.

CRediT authorship contribution statement

Lorenza Fagnani: Writing – review & editing, Writing – original draft, Methodology, Investigation, Formal analysis, Conceptualization. **Pierangelo Bellio:** Methodology, Investigation, Conceptualization. **Antonio Di Giulio:** Writing – review & editing, Supervision. **Lisaurora Nazzicone:** Investigation. **Roberto Iorio:** Investigation, Formal analysis. **Sabrina Petricca:** Investigation. **Nicola Franceschini:** Supervision, Resources. **Laura Bertarini:** Investigation, Formal analysis. **Donatella Tondi:** Writing – review & editing, Formal analysis. **Giuseppe Celenza:** Supervision, Resources, Funding acquisition, Formal analysis, Conceptualization.

Declaration of competing interest

The authors declare that they have no known competing financial interests or personal relationships that could have appeared to influence the work reported in this paper.

Acknowledgements

This research received no external funding. The authors would like to thank Marisa Piovano (Universidad Técnica Federico Santa María) for providing the pure substances.

Appendix A. Supplementary data

Supplementary data to this article can be found online at https://doi.org/10.1016/j.heliyon.2024.e38445.

References

[1] Liang, P.-H. Characterization and inhibition of SARS-coronavirus main protease. Curr. Top. Med. Chem. 6 (4), 361–376.
[2] Anand, K.; Ziebuhr, J.; Wadhwani, P.; Mesters, J. R.; Hilgenfeld, R. Coronavirus main proteinase (3CLpro) structure: basis for design of anti-SARS drugs. Science 300 (5626), 1763–1767.
[3] Kuiken, T.; Fouchier, R. A. M.; Schutten, M.; Rimmelzwaan, G. F.; van Amerongen, G.; van Riel, D.; Laman, J. D.; de Jong, T.; van Doornum, G.; Lim, W.; Ling, A. E.; Chan, P. K. S.; Tam, J. S.; Zambon, M. C.; Gopal, R.; Drosten, C.; van der Werf, S.; Escriou, N.; Manuguerra, J.-C.; Stöhr, K.; Peiris, J. S. M.; Osterhaus, A. D. M. E. Newly discovered coronavirus as the primary cause of severe acute respiratory syndrome. Lancet 362 (9380), 263–270.
[4] Drosten, C.; Günther, S.; Preiser, W.; van der Werf, S.; Brodt, H.-R.; Becker, S.; Rabenau, H.; Panning, M.; Kolesnikova, L.; Fouchier, R. A. M.; Berger, A.; Burguière, A.-M.; Cinatl, J.; Eickmann, M.; Escriou, N.; Grywna, K.; Kramme, S.; Manuguerra, J.-C.; Müller, S.; Rickerts, V.; Stürmer, M.; Vieth, S.; Klenk, H.-D.; Osterhaus, A. D. M. E.; Schmitz, H.; Doerr, H. W. Identification of a novel coronavirus in patients with severe acute respiratory syndrome. N. Engl. J. Med. 348 (20), 1967–1976.
[5] Fouchier, R. A. M.; Kuiken, T.; Schutten, M.; van Amerongen, G.; van Doornum, G. J. J.; van den Hoogen, B. G.; Peiris, M.; Lim, W.; Stöhr, K.; Osterhaus, A. D. M. E. Koch's postulates fulfilled for SARS virus. Nature 423 (6937), 240–240.
[6] Ksiazek, T. G.; Erdman, D.; Goldsmith, C. S.; Zaki, S. R.; Peret, T.; Emery, S.; Tong, S.; Urbani, C.; Comer, J. A.; Lim, W.; Rollin, P. E.; Dowell, S. F.; Ling, A.-E.; Humphrey, C. D.; Shieh, W.-J.; Guarner, J.; Paddock, C. D.; Rota, P.; Fields, B.; DeRisi, J.; Yang, J.-Y.; Cox, N.; Hughes, J. M.; LeDuc, J. W.; Bellini, W. J.; Anderson, L. J.; SARS working group. A novel coronavirus associated with severe acute respiratory syndrome. N. Engl. J. Med. 348 (20), 1953–1966.
[7] Coronavirus Disease (COVID-19) – World Health Organization.
[8] Goyal, B.; Goyal, D. Targeting the dimerization of the main protease of coronaviruses: a potential broad-spectrum therapeutic strategy. ACS Comb. Sci. 22 (6), 297–305.
[9] Majumdar, M.; Singh, V.; Misra, T. K.; Roy, D. N. In silico studies on structural inhibition of SARS-CoV-2 main protease Mpro by major secondary metabolites of andrographis paniculata and cinchona officinalis. Biologia (Bratisl) 77 (5), 1373–1389.
[10] Song, Z.; Xu, Y.; Bao, L.; Zhang, L.; Yu, P.; Qu, Y.; Zhu, H.; Zhao, W.; Han, Y.; Qin, C. From SARS to MERS, thrusting coronaviruses into the spotlight. Viruses 11 (1), 59.
[11] Zhang, L.; Lin, D.; Sun, X.; Curth, U.; Drosten, C.; Sauerhering, L.; Becker, S.; Rox, K.; Hilgenfeld, R. Crystal structure of SARS-CoV-2 main protease provides a basis for design of improved α-ketoamide inhibitors. Science 368 (6489), 409–412.
[12] Goyal, R.; Gautam, R. K.; Chopra, H.; Dubey, A. K.; Singla, R. K.; Rayan, R. A.; Kamal, M. A. Comparative highlights on MERS-CoV, SARS-CoV-1, SARS-CoV-2, and NEO-CoV. EXCLI J 21, 1245–1272.
[13] de Wit, E.; van Doremalen, N.; Falzarano, D.; Munster, V. J. SARS and MERS: recent insights into emerging coronaviruses. Nat. Rev. Microbiol. 14 (8), 523–534.
[14] Zhou, P.; Yang, X.-L.; Wang, X.-G.; Hu, B.; Zhang, L.; Zhang, W.; Si, H.-R.; Zhu, Y.; Li, B.; Huang, C.-L.; Chen, H.-D.; Chen, J.; Luo, Y.; Guo, H.; Jiang, R.-D.; Liu, M.-Q.; Chen, Y.; Shen, X.-R.; Wang, X.; Zheng, X.-S.; Zhao, K.; Chen, Q.-J.; Deng, F.; Liu, L.-L.; Yan, B.; Zhan, F.-X.; Wang, Y.-Y.; Xiao, G.-F.; Shi, Z.-L. A pneumonia outbreak associated with a new coronavirus of probable bat origin. Nature 579 (7798), 270–273.
[15] Mahase, E. Covid-19: pfizer's Paxlovid is 89% effective in patients at risk of serious illness, company reports. BMJ 375, n2713.
[16] Goyal, B.; Goyal, D. Targeting the dimerization of the main protease of coronaviruses: a potential broad-spectrum therapeutic strategy. ACS Comb. Sci. 22 (6), 297–305.
[17] Celenza, G.; Segatore, B.; Setacci, D.; Perilli, M.; Brisdelli, F.; Bellio, P.; Piovano, M.; Garbarino, J. A.; Amicosante, G.; Nicoletti, M. Antibacterial activity of selected metabolites from Chilean lichen species against methicillin-resistant staphylococci. Nat. Prod. Res. 27 (17), 1528–1531.
[18] Astuti, I.; Ysrafil, null. Severe acute respiratory syndrome coronavirus 2 (SARS-CoV-2): an overview of viral structure and host response. Diabetes Metabol. Syndr. 14 (4), 407–412.
[19] Desmarets, L.; Millot, M.; Chollet-Krugler, M.; Boustie, J.; Camuzet, C.; François, N.; Rouillé, Y.; Belouzard, S.; Tomasi, S.; Mambu, L.; Séron, K. Lichen or associated micro-organism compounds are active against human coronaviruses. Viruses 15 (9), 1859.

[20] Fagnani, L.; Nazzicone, L.; Bellio, P.; Franceschini, N.; Tondi, D.; Verri, A.; Petricca, S.; Iorio, R.; Amicosante, G.; Perilli, M.; Celenza, G. Protocetraric and salazinic acids as potential inhibitors of SARS-CoV-2 3CL protease: biochemical, cytotoxic, and computational characterization of depsidones as slow-binding inactivators. Pharmaceuticals 15 (6), 714.
[21] Morrison, J. F.; Walsh, C. T. The behavior and significance of slow-binding enzyme inhibitors. Adv. Enzymol. Relat. Area Mol. Biol. 61, 201–301.
[22] Ferreira, J. C.; Fadl, S.; Rabeh, W. M. Key dimer interface residues impact the catalytic activity of 3CLpro, the main protease of SARS-CoV-2. J. Biol. Chem. 298 (6), 102023.
[23] Wei, P.; Fan, K.; Chen, H.; Ma, L.; Huang, C.; Tan, L.; Xi, D.; Li, C.; Liu, Y.; Cao, A.; Lai, L. The N-terminal octapeptide acts as a dimerization inhibitor of SARS coronavirus 3C-like proteinase. Biochem. Biophys. Res. Commun. 339 (3), 865–872.
[24] Chou, C.-Y.; Chang, H.-C.; Hsu, W.-C.; Lin, T.-Z.; Lin, C.-H.; Chang, G.-G. Quaternary structure of the severe acute respiratory syndrome (SARS) coronavirus main protease. Biochemistry 43 (47), 14958–14970.
[25] Gan, C.; Jia, X.; Fan, S.; Wang, S.; Jing, W.; Wei, X. Virtual screening and molecular dynamics simulation to identify potential SARS-CoV-2 3CLpro inhibitors from a natural product compounds library. Acta Virol. 67, 12464.
[26] Tam, N. M.; Pham, D.-H.; Hiep, D. M.; Tran, P.-T.; Quang, D. T.; Ngo, S. T. Searching and designing potential inhibitors for SARS-CoV-2 Mpro from natural sources using atomistic and deep-learning calculations. RSC Adv. 11 (61), 38495–38504.
[27] Liu, N.; Yang, Z.; Liu, Y.; Dang, X.; Zhang, Q.; Wang, J.; Liu, X.; Zhang, J.; Pan, X. Identification of a putative SARS-CoV-2 main protease inhibitor through in silico screening of self-designed molecular library. Int. J. Mol. Sci. 24 (14), 11390.
[28] Pennisi, R.; Gentile, D.; Rescifina, A.; Napoli, E.; Trischitta, P.; Piperno, A.; Sciortino, M. T. An integrated in silico and in vitro approach for the identification of natural products active against SARS-CoV-2. Biomolecules 14 (1), 43.
[29] Wang, G.; Venegas, F. A.; Rueda, A. M.; Weerasinghe, N. W.; Uggowitzer, K. A.; Thibodeaux, C. J.; Moitessier, N.; Mittermaier, A. K. A naturally occurring G11S mutation in the 3C-like protease from the SARS-CoV-2 virus dramatically weakens the dimer interface. Protein Sci. 33 (1), e4857.
[30] Zhang, Y.-N.; Zhu, G.-H.; Liu, W.; Xiong, Y.; Hu, Q.; Zhuang, X.-Y.; Jia, G.-H.; Zhang, W.-D.; Ge, G.-B. Discovery and characterization of the covalent SARS-CoV-2 3CLpro inhibitors from Ginkgo biloba extract via integrating chemoproteomic and biochemical approaches. Phytomedicine 114, 154796.
[31] Hicks, E. G.; Kandel, S. E.; Lampe, J. N. Identification of aloe-derived natural products as prospective lead scaffolds for SARS-CoV-2 main protease (Mpro) inhibitors. Bioorg. Med. Chem. Lett. 66, 128732.
[32] Panagiotopoulos, A. A.; Karakasiliotis, I.; Kotzampasi, D.-M.; Dimitriou, M.; Sourvinos, G.; Kampa, M.; Pirintsos, S.; Castanas, E.; Daskalakis, V. Natural polyphenols inhibit the dimerization of the SARS-CoV-2 main protease: the case of fortunellin and its structural analogs. Molecules 26 (19), 6068.
[33] Cheng, S.-C.; Chang, G.-G.; Chou, C.-Y. Mutation of glu-166 blocks the substrate-induced dimerization of SARS coronavirus main protease. Biophys. J. 98 (7), 1327–1336.
[34] Ureña-Vacas, I.; González-Burgos, E.; Divakar, P. K.; Gómez-Serranillos, M. P. Lichen depsidones with biological interest. Planta Med. 88 (11), 855–880.
[35] Ingelfinger, R.; Henke, M.; Roser, L.; Ulshöfer, T.; Calchera, A.; Singh, G.; Parnham, M. J.; Geisslinger, G.; Fürst, R.; Schmitt, I.; Schiffmann, S. Unraveling the pharmacological potential of lichen extracts in the context of cancer and inflammation with a broad screening approach. Front. Pharmacol. 11, 1322.
[36] Coelho, L. C. Antimicrobial Activity of Secondary Metabolites and Lectins from Plants. 396–406.
[37] Bellio, P.; Di Pietro, L.; Mancini, A.; Piovano, M.; Nicoletti, M.; Brisdelli, F.; Tondi, D.; Cendron, L.; Franceschini, N.; Amicosante, G.; Perilli, M.; Celenza, G. SOS response in bacteria: inhibitory activity of lichen secondary metabolites against Escherichia coli RecA protein. Phytomedicine 29, 11–18.
[38] Kuzmič, P. DynaFit–a software package for enzymology. Methods Enzymol. 467, 247–280.
[39] Ghosh, A. K.; Raghavaiah, J.; Shahabi, D.; Yadav, M.; Anson, B. J.; Lendy, E. K.; Hattori, S.; Higashi-Kuwata, N.; Mitsuya, H.; Mesecar, A. D. Indole Chloropyridinyl ester-derived SARS-CoV-2 3CLpro inhibitors: enzyme inhibition, antiviral efficacy, structure–activity relationship, and X-ray structural studies. J. Med. Chem. 64 (19), 14702–14714.